Acta Pharmaceutica Sinica B 2024;14(12):5493−5504

Chinese Pharmaceutical Association
Institute of Materia Medica, Chinese Academy of Medical Sciences

Acta Pharmaceutica Sinica B

www.elsevier.com/locate/apsb
www.sciencedirect.com

SHORT COMMUNICATION

Discovery of a novel exceptionally potent and orally active Nur77 ligand NB1 with a distinct binding mode for cancer therapy

Jun Chen [a,†], Taige Zhao [a,†], Wenbin Hong [b,†], Hongsheng Li [a], Mingtao Ao [a,e], Yijing Zhong [a], Xiaoya Chen [a], Yingkun Qiu [a], Xiumin Wang [a], Zhen Wu [a], Tianwei Lin [d], Baicun Li [c,*], Xueqin Chen [b,*], Meijuan Fang [a,*]

[a]*State Key Laboratory of Cellular Stress Biology and Fujian Provincial Key Laboratory of Innovative Drug Target Research, School of Pharmaceutical Science, Xiamen University, Xiamen 361102, China*
[b]*Xiamen Key Laboratory of Clinical Efficacy and Evidence Studies of Traditional Chinese Medicine, the First Affiliated Hospital of Xiamen University, School of Medicine, Xiamen University, Xiamen 361003, China*
[c]*Center of Respiratory Medicine, China-Japan Friendship Hospital, National Center for Respiratory Medicine, Institute of Respiratory Medicine, Chinese Academy of Medical Sciences, National Clinical Research Center for Respiratory Diseases, State Key Laboratory of Respiratory Health and Multimorbidity, Beijing 100029, China*
[d]*School of Life Sciences, Xiamen University, Xiamen 361102, China*
[e]*School of Pharmacy, Hubei University of Science and Technology, Xianning 437100, China*

Received 25 March 2024; received in revised form 3 June 2024; accepted 4 July 2024

KEY WORDS

Novel Nur77 ligand;
4,4′-Bipyridine cinnamamide derivatives;
X-ray crystallography;
Nur77/Bcl-2 apoptotic pathway;
Anticancer activity

Abstract The orphan nuclear receptor Nur77 is emerging as an attractive target for cancer therapy, and activating Nur77's non-genotypic anticancer function has demonstrated strong therapeutic potential. However, few Nur77 site B ligands have been identified as excellent anticancer compounds. There are no co-crystal structures of effective anticancer agents at Nur77 site B, which greatly limits the development of novel Nur77 site B ligands. Moreover, the lack of pharmaceutical ligands restricts Nur77's therapeutic proof of concept. Herein, we developed a first-in-class Nur77 site B ligand (NB1) that significantly inhibited cancer cells by mediating the Nur77/Bcl-2-related apoptotic effect at mitochondria. The X-ray crystallography suggests that NB1 is bound to the Nur77 site B with a distinct binding mode. Importantly, NB1 showed favorable pharmacokinetic profiles and safety, as evidenced by

*Corresponding authors.
E-mail addresses: lbc19890303@126.com (Baicun Li), xqchen@xmu.edu.cn (Xueqin Chen), fangmj@xmu.edu.cn (Meijuan Fang).
†These authors made equal contributions to this work.
Peer review under the responsibility of Chinese Pharmaceutical Association and Institute of Materia Medica, Chinese Academy of Medical Sciences.

https://doi.org/10.1016/j.apsb.2024.07.012

its good oral bioavailability in rats and lack of mortality, bodyweight loss, and pathological damage at the 512.0 mg/kg dose in mice. Furthermore, oral administration of NB1 demonstrated remarkable *in vivo* anticancer efficacy in an MDA-MB-231 xenograft model. Together, our work discovers NB1 as a new generation Nur77 ligand that activates the Nur77/Bcl-2 apoptotic pathway with a safe and effective cancer therapeutic potency.

1. Introduction

Nur77 (also known as TR3 and NGFI-B) is nuclear receptor subfamily 4 group A member 1 (NR4A1)[1-4]. In general, it acts as a transcription factor localized in the nucleus to regulate the expression of target genes (*e.g.*, ITGB1, PD-L1, WFDC21P) by binding to different transcription cofactors (*e.g.*, Sp1 and p300)[5-8]. In addition, Nur77 is an immediate-early gene that can rapidly respond to external stimuli and export from the nucleus to the cytoplasm, exerting its non-genomic activity[9,10]. Notably, multiple studies have demonstrated that Nur77 has an essential contribution to the progression of various types of cancer due to its critical roles in the metabolism[11], proliferation[12], apoptosis[13], and invasion[14] of tumor cells, as well as tumor immunity[15] and tumor angiogenesis[16-18]. In particular, dysregulation of Nur77 has also been observed in solid tumors and is significantly associated with poor patient prognosis[19]. Excitingly, increasing studies have demonstrated that the subcellular localization of Nur77 targeting mitochondria or endoplasmic reticulum (ER) can initiate cancer cell apoptosis, effectively inhibiting tumor growth *in vitro* and *in vivo*[20-23]. For instance, Nur77 can localize to mitochondria, interacting with the LOOP of the classic pro-survival protein Bcl-2 and changing Bcl-2's conformation to pro-apoptotic protein, promoting apoptosis of cancer cells[9,24]. Recently, targeting Nur77's non-genomic activity to induce cell death has emerged as a potentially effective therapy for malignant tumors[25-28].

Although the endogenous ligand of Nur77 has not yet been found, several categories of chemical entities have been reported to target regulating the various biological functions of Nur77[7,8,23,29-35]. Notably, most Nur77 modulators showed significant therapeutic potency in cancer treatment, especially for those small molecules inducing Nur77 nuclear translocation. For instance, BI1071[31], Celastrol[32,36], and our compounds **8b**[33] and **ja**[34] were found to mediate Nur77 translocation from the nucleus into mitochondria, causing cell apoptosis. THPN can stimulate the interaction of Nur77 and mitochondrial outer membrane protein Nix to translocate Nur77 to mitochondria, ultimately leading to autophagic cell death due to the dissipation of mitochondrial membrane potential[35]. Besides, **10g** could mediate Nur77 subcellular localization to induce endoplasmic reticulum stress, thereby promoting cell autophagy and apoptosis[23]. However, no drug candidate targeting Nur77 has been developed in clinical trials, which might be because the reported compounds exhibit toxicity, lack of oral absorption, or have other undesirable druggable properties[27,33,37]. Therefore, developing novel Nur77 ligands with favorable drug properties is crucial and beneficial to the clinical treatment of cancers.

The previously reported co-crystal structures of Nur77 with Csn-B and its derivatives [8,18,30,32,33] have revealed several potential binding sites of Nur77 ligand binding domain ($Nur77^{LBD}$), including binding sites A[30], B[30], C[18], D[8], and so on. Interestingly, when we utilized the CavityPlus[38,39] to detect potential binding site in $Nur77^{LBD}$ (PDB ID: 3V3E), the CAVITY program output eight cavities, and three cavities named Cavity_1 (the binding site C), Cavity_2 (the binding site B), and Cavity_4 were predicted to be druggable (Supporting Information Fig. S1 and Table S1). Interestingly, several active compounds (*e.g.*, BI1071[31] and XS561[40]) have also been demonstrated as Nur77 site B ligands with excellent *in vivo* anticancer activities. These findings implied that binding site B is an attractive druggable binding site of $Nur77^{LBD}$, and it is fascinating to discover novel Nur77 ligands at binding site B for treating cancer. Therefore, developing novel $Nur77^{LBD}$ site B ligands with favorable druggability is crucial and beneficial to the clinical treatment of cancers. However, there are no co-crystals of effective anticancer compounds with $Nur77^{LBD}$ at binding site B, impeding the development of pharmaceutical Nur77 site B ligands.

Encouragingly, in search of new Nur77 ligands in our in-house compound library, compound BPA-B9 was found to be a first-in-class Nur77 ligand (K_D = 0.46 μmol/L), and it displayed excellent binding affinity of $Nur77^{LBD}$ at site B in molecular docking study. Moreover, a series of potential Nur77 site B ligands were designed and synthesized based on the predicted binding mode of BPA-B9 with Nur77 at binding site B. Among the synthesized compounds, NB1 showed the most potency against tested cancer cell lines, which was superior/equipotent to those of the lead compound BPA-B9. Excitedly, NB1 displayed higher *in vitro* Nur77 selectivity than other tested nuclear receptors (including RXRα, ERα, ERβ, and PPARγ), and the X-ray crystallography revealed its distinct binding mode at the binding site B of Nur77. Importantly, NB1 was an orally available and highly potent new-generation Nur77 ligand that exhibited excellent anticancer efficacy in the MDA-MB-231 xenograft model.

2. Results and discussion

2.1. Compound design and synthesis

Recently, we screened the in-house compound library to identify new potential Nur77 ligands for hit-to-lead development. Fortunately, 4,4′-bipyridine amide derivative BPA-B9 was found to be a good Nur77 binder with a K_D (equilibrium dissociation constant) value of 0.46 μmol/L (Fig. 1A and B). Also, BPA-B9 significantly inhibited the Nur77-driven luciferase activity at the concentrations of 62.5 and 125.0 nmol/L, demonstrating its Nur77-binding ability in cells (Fig. 1C). Subsequently, we conducted induced-fit docking (IFD) analysis to investigate whether and how BPA-B9 docked to the binding site B of $Nur77^{LBD}$ (PDB code: 3V3Q)[41]. The result showed that BPA-B9, like a dragon molecule, occupied the binding site B with a docking value of −10.336 kcal/mol

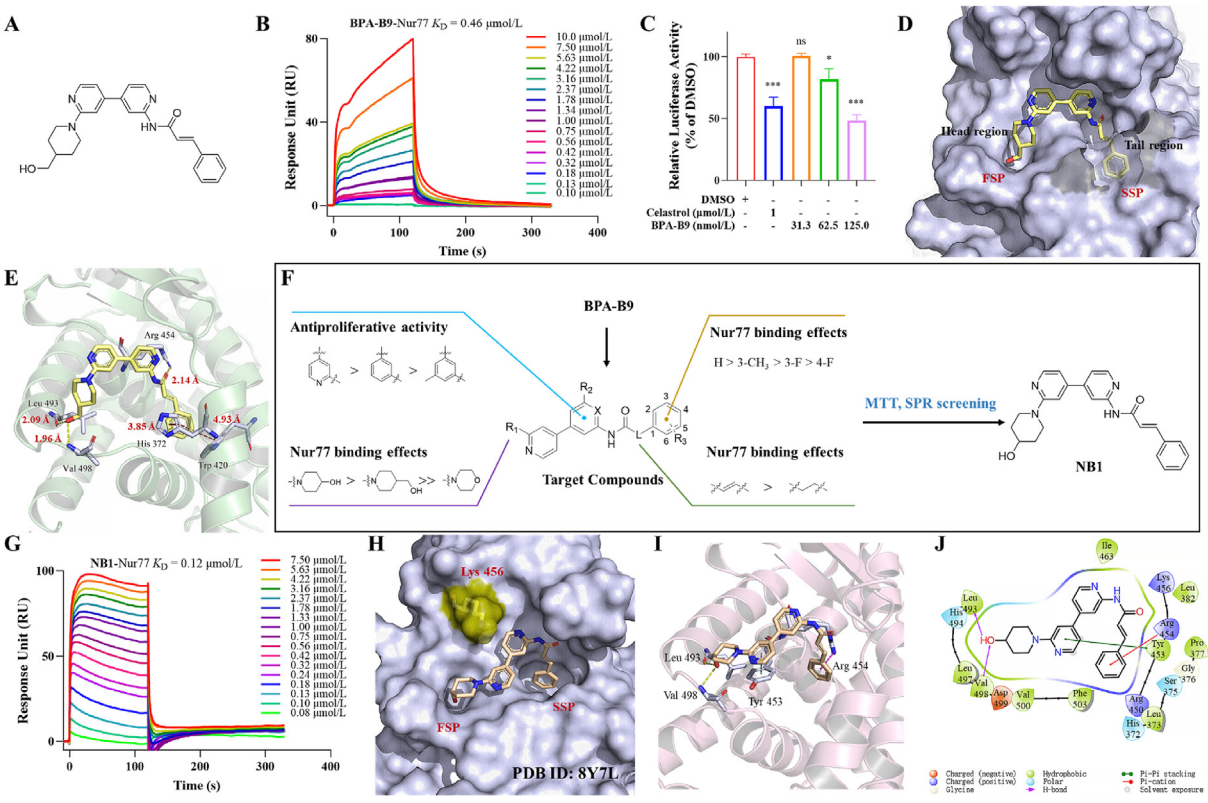

Figure 1 The novel Nur77 ligand NB1 derived from the lead BPA-B9 (NA1) shows a distinct binding mode at Nur77^{LBD} binding site B. (A) Chemical structure of BPA-B9. (B) SPR analysis of BPA-B9 binding to Nur77^{LBD}. (C) HeLa cells co-transfected with pG5-Luciferase and pBind-Nur77-LBD plasmids were treated with BPA-B9 at different action concentrations for 24 h. Celastrol was used as a positive control to Nur77. Data are shown as mean ± SD. Ns, not significant, $0.01< *P < 0.05$, $***P < 0.001$ *vs.* control (DMSO). (D) The binding mode of BPA-B9 to Nur77^{LBD}. BPA-B9 was represented as a yellow carbon stick, and Nur77^{LBD} was shown as a blue-white surface. (E) 3D interaction diagram of BPA-B9 with Nur77^{LBD}. BPA-B9 was displayed as a yellow carbon stick, and the key residues were shown as blue-white sticks. (F) The scheme of designing and screening novel anti-tumor small molecules targeting Nur77^{LBD}. (G) SPR analysis of NB1 binding to Nur77^{LBD}. (H) The newly released crystal structure of NB1 in complex with Nur77^{LBD} protein (PDB ID: 8Y7L). The protein was represented as a blue-white surface, and NB1 was shown as a wheat stick. (I) The 3D interaction diagram of NB1 with Nur77^{LBD}. NB1 was displayed as a wheat stick, and the key residues were shown as blue-white sticks. (J) The 2D binding model of NB1 and Nur77^{LBD}.

(Fig. 1D). Clearly, there were three main interactions between BPA-B9 and the binding site B of Nur77^{LBD} (Fig. 1E). First, the 4-(hydroxymethyl)piperidin-1-yl moiety (head anchor) as a dragon head was effectively positioned within the first sub-pocket (FSP) in the head region, and its hydroxyl group formed two hydrogen bonds with the backbone carbonyl oxygen (2.09 Å) and amino hydrogen (1.96 Å) of Leu493 and Val498, respectively. Second, the phenyl group as a dragon tail (caudal hook) well fitted into the second sub-pocket (SSP) in the tail region, and it formed two $\pi-\pi$ stacking interactions with residues Trp420 and His372. Third, the linker's carbonyl oxygen as a dragon body forms the "signature" hydrogen bond (2.14 Å) with the residue of Arg454. Together, BPA-B9 was a new chemotype targeting Nur77 and provided a potential starting scaffold for structural optimization to improve target selectivity, biological activities, and physicochemical properties. To develop new Nur77 site B ligands with improved target selectivity and druggability, we therefore made appropriate modifications of BPA-B9 (NA1) (Fig. 1F). For the head anchor, the 4-(hydroxymethyl)piperidin-1-yl moiety (R_1) was changed to similar polar groups (4-hydroxypiperidin-1-yl and morpholino). Besides, the scaffold 4,4′-bipyridine was replaced with similar aromatic fragments, including 4-methyl-3,4′-bipyridine 5-methyl-3,4′-bipyridine and 4-(*m*-tolyl)pyridine. Furthermore, the ethyl linker (L) was utilized to improve the rigid structure and explore the importance of the vinyl chain on the activity. Finally, the influence of introducing −F or $-CH_3$ on C-3 or C-4 positions of the benzene ring on the activity since the space around the benzene ring in the SSP was tiny. As previously reported[42], twenty target compounds were first synthesized according to the procedures outlined in Supporting Information Schemes S1 and S2.

2.2. *In vitro anticancer activity and Nur77-binding affinity evaluation*

All synthesized compounds at 5.0 μmol/L were first screened for cytotoxicity towards three cancer cell lines (HeLa, MDA-MB-231, and A549)[7,14,31]. Concurrently, the initial surface plasmon resonance (SPR) experiment was conducted to test the binding response unit (RU) of the compounds to Nur77^{LBD} at a concentration of 10.0 μmol/L. The compound screening results were summarized in Supporting Information Tables S2 and S3. The preliminary structure−activity relationships (SARs) of the entitled compounds were furnished based on the anti-proliferative and Nur77-binding activities, as illustrated in Fig. 1F. The scaffold B

ring played a crucial role in the anti-proliferative activity. Replacing the pyridine scaffold with a benzene ring generally reduced anti-proliferative activities (NA1 *vs.* NA3, NB1 *vs.* NB3, and NC1 *vs.* NC3). Moreover, introducing methyl group at R_2 of benzene scaffold generally resulted in a further loss in anti-proliferative activities (*e.g.*, NB3 *vs.* NB5 and NC3 *vs.* NC5). Additionally, R_1 and R_2 substituents and the linker L showed great impacts on the Nur77-binding effects. For R_1 group, the replacement of 4-(hydroxymethyl)piperidin-1-yl with 2-(4-hydroxypiperidin-1-yl)pyridin-4-yl (NA1 *vs.* NB1)) increased the Nur77-binding activity, while replacing the 4-(hydroxymethyl) piperidin-1-yl with morpholino (NC1) significantly reduced the Nur77-binding activity. Introducing substituents $-CH_3$ and $-F$ at C-3′ or C-4′ positions of the phenyl ring (NB2, NB1a, and NB1b: RU $<$ 45) showed a remarkable decrease in the Nur77-binding activity as compared to NB1 (RU = 100.69). Moreover, the replacement of the vinyl moiety by a flexible ethyl group in the linker (NB1c-NB1e: RU $<$ 26) drastically reduced the Nur77-binding activity. Together, the 2,4-disubstituted pyridine ring (for scaffold A), the vinyl chain (for L linker), and the phenyl group (for B-ring) might be optimal for Nur77-binding affinity. Based on the obtained data, the most active compound, NB1, was selected for further studies.

2.3. *NB1 is a novel selective Nur77 site B ligand with excellent anticancer activity*

First, NB1 was assessed for further anticancer activity and Nur77-binding selectivity. As shown in Table 1, NB1 exhibited the best inhibition on triple-negative breast cancer (TNBC) MDA-MB-231 cells (IC_{50} = 0.0030 ± 0.0015 μmol/L). Also, NB1 displayed potent anti-proliferative activity with IC_{50} values in the nano-molar against most other test cancer cell lines, such as A549 (IC_{50} = 0.0850 ± 0.0080 μmol/L), HeLa (IC_{50} = 0.0741 ± 0.0066 μmol/L), HepG2 (IC_{50} = 0.1105 ± 0.0070 μmol/L), and HCC1937 (IC_{50} = 0.5277 ± 0.2068 μmol/L). In particular, the inhibitory potency of NB1 against MDA-MB-231 and A549 cells was superior to that of the lead compound NA1 (Supporting Information Table S4). Notably, NB1 showed low anti-proliferative activities against MCF-7 (non-TNBC, IC_{50} = 2.5110 ± 0.3792 μmol/L) and human normal breast MCF-10A cells (IC_{50} = 3.3330 ± 0.2447 μmol/L) with selective indexes of 837 and 1111, respectively (compared to MDA-MB-231). These findings manifested that Nur77 ligand NB1 was an excellent anticancer agent *in vitro*. Importantly, SPR assay demonstrated that NB1 had better binding affinities to Nur77 (K_D = 0.12 μmol/L) than other tested nuclear receptors (SI ≥ 6.5), including RXRα, ERα, ERβ, and PPARγ (Fig. 1G, Table 1, and Supporting Information Fig. S2A−D).

To define the binding mode of NB1, we then conducted crystallographic studies on its complexes of $Nur77^{LBD}$ protein. The obtained co-crystals of the NB1/$Nur77^{LBD}$ complex were solved by the molecular-replacement method and were refined satisfactorily (Fig. S2E and Supporting Information Tables S5). The crystal structure of the NB1/$Nur77^{LBD}$ complex was determined at a 2.68 Å resolution. As shown in Fig. 1H, NB1 occupied the binding site B of $Nur77^{LBD}$ and exhibited a similar binding pose with the predicted conformation of the lead NA1. The hydroxypiperazine moiety made the hydrogen bond interactions with Leu493 and Val 498 in the FSP, while the phenyl moiety occupied the SSP and formed $\pi-\pi$ stacking interaction with Arg454 (Fig. 1I and J). Besides, the 4,4′-bipyridyl scaffold is well positioned to make additional $\pi-\pi$ stacking interactions with Tyr453. Nevertheless, it should be pointed out that the gatekeeper Lys456 could hinder the substituted 4,4′-bipyridyl scaffold occupies the solvent-exposed groove (Fig. 1H). Notably, the unsaturated olefin chain in the NB1 structure was also an essential supportive backbone, and its trans conformation ensured the benzene ring perfectly fit into the SSP. Meanwhile, the volume size of SSP is precisely adequate to accommodate an unsubstituted benzene ring. Interestingly, the complex structure of the NB1 bounded Nur77 LBD was with complete electron density at amino acids residues Val391 to Lys396 compared to apo-$Nur77^{LBD}$ (Fig. S2F), suggesting that NB1 stabilized the $Nur77^{LBD}$ conformation, which may contribute to its excellent biological function.

2.4. *NB1 inhibits cell proliferation by inducing mitotic arrest and cell apoptosis*

To elucidate NB1's anticancer action, we then determined changes in gene expression between DMSO and 250.0 nmol/L NB1-treated MDA-MB-231 cells by RNA-Seq analysis. In total, expression levels of 15,258 and 15,313 annotated human genes (being 14,719 same genes) were detected in the control and NB1-treated groups, respectively (Fig. 2A). Among them, 288 genes (q-value $<$0.05, $|\text{Log}_2(\text{Fold Change})| > 0.5$) were identified as differentially expressed genes (DEGs), including up-regulated 124 genes and down-regulated 164 genes (Fig. 2B). Gene Ontology Biology Process (GOBP) analysis indicated NB1 mainly participated in

Table 1 The cell inhibitory activities and nuclear receptor-binding affinities of NB1.

Cell inhibitory activity			Binding affinity	
Cell line	IC_{50} (μmol/L)[a]	SI[b]	Nuclear receptor	K_D[c] (SI[d])
MDA-MB-231	0.0030 ± 0.0015	1.00	Nur77	0.12 μmol/L
HCC1937	0.5277 ± 0.2068	175.90	RXRα	0.78 μmol/L (6.50)
MCF-7	2.5110 ± 0.3792	837.00	ERα	1.28 μmol/L (10.67)
A549	0.0850 ± 0.0080	28.33	ERβ	1.63 μmol/L (13.58)
HeLa	0.0741 ± 0.0066	24.70	PPARγ	1.35 μmol/L (11.25)
HepG2	0.1105 ± 0.0070	36.83		
MCF-10A	3.3330 ± 0.2447	1111.00		

[a]Data are mean ± SD of three independent determinations.
[b]SI: the ratio of the IC_{50} values of NB1 in other cell lines divided by the IC_{50} values in MDA-MB-231.
[c]The K_D was determined in concentration gradients of the target compounds by SPR assay.
[d]SI: the ratio of the K_D values of target compounds binding to other nuclear receptors divided by the K_D values to Nur77.

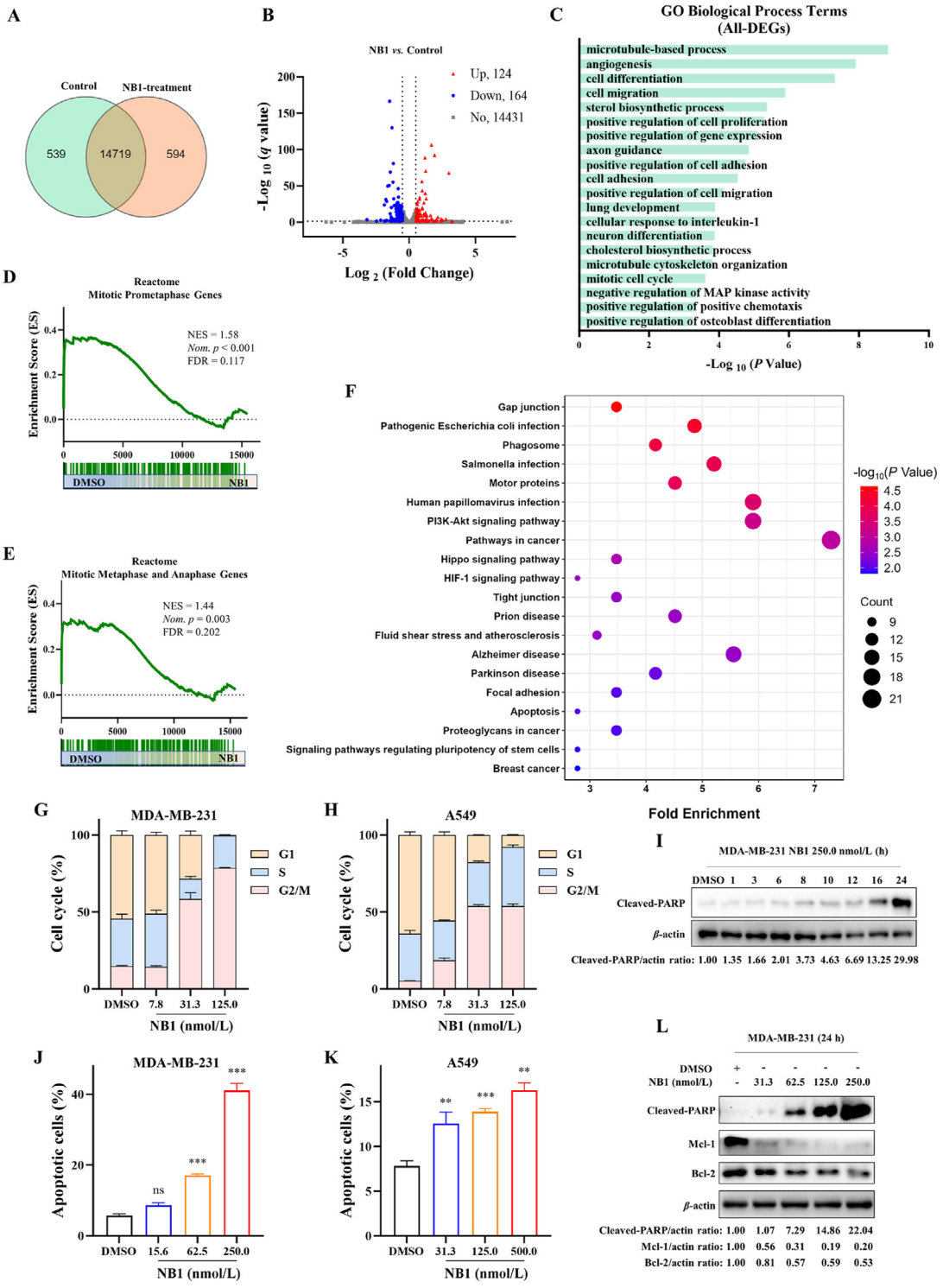

Figure 2 NB1 triggered cell cycle arrest and apoptosis in cancer cells. (A) The annotated human genes in DMSO- and NB1-treated MDA-MB-231 cells. (B) Visualization of differential genes by volcano plot of MDA-MB-231 cells treated with NB1 for 12 h ($n = 3$). Red points for up-regulated genes, blue for down-regulated genes, and gray for unchanged genes ($|\text{Log}_2(\text{Fold Change})| > 0.5$, q value < 0.05). (C) Top 20 biological processes enriched by GO database at NB1. (D, E) Gene set enrichment analysis (GSEA) revealed the influence of NB1 on the mitotic gene signature in MDA-MB-231 cells. NES, normalized enrichment score; FDR, false discovery rate; *Nom.*, nominal. (F) Top 20 pathway terms enriched by KEGG database in NB1-treated cells. (G, H) The ability of NB1 to induce mitotic arrest in MDA-MB-231 (G) and A549 (H) cells. (I) Western blot analyzed the expression of cleaved-PARP in MDA-MB-231 cells treated with 250.0 nmol/L NB1 for indicated time. (J, K) The ability of NB1 to induce apoptosis in MDA-MB-231 (J) and A549 (K) cells. (L) Western blot showed that NB1 affected the expression of cleaved-PARP, Bcl-2, and Mcl-1. Data are shown as mean ± SD. Ns, not significant, $0.001 < **P < 0.01$, $***P < 0.001$ *vs.* control (DMSO).

crucial pathways of cell mitosis, including "microtubule-based process" (10 genes, P = 1.47e-09), "microtubule cytoskeleton organization" (22 genes, P = 1.57e-04), and "mitotic cell cycle" (10 genes, P = 2.46e-04) (Fig. 2C). Further, the separate GOBP enrichment analyses for the up-regulated and down-regulated DEGs implied that NB1 primarily suppressed the expression of mitotic cell cycle-related genes and increased the expression of genes involved in the apoptotic process (Supporting Information Fig. S3A and B). Simultaneously, Gene Set Enrichment Analyses (GSEA) analysis also showed that a prominent reduction in mitotic process gene signature was observed in MDA-MB-231 cells treated with NB1 (Fig. 2D–E). Additionally, the KEGG analysis of the identified DEGs implied that the apoptosis, PI3K-AKT, and HIF-1 signaling pathways were the primary ones distinctly affected by NB1 treatment (P-value <0.05) (Fig. 2F and Supporting Information Material II). These findings suggested that NB1 might disturb cell mitosis and apoptosis processes of cancer cells.

Subsequently, the flow cytometry assay was conducted to examine the cell cycle distribution of A549 and MDA-MB-231 cells with DMSO or NB1 treatment. As shown in Fig. 2G and H, NB1 significantly induced G2/M phase cell cycle arrest in A549 and MDA-MB-231 cells. In DMSO-treated MDA-MB-231 cells, the population of cells in the G2/M phase was 14.82%. After treating NB1 at 7.8, 31.3, and 125.0 nmol/L for 12 h, the fraction of MDA-MB-231 cells in the G2/M phase was 14.44%, 58.39%, and 78.55%, respectively. After incubation with NB1 at 7.8, 31.3, and 125.0 nmol/L for 12 h, the percentage of A549 cells in the G2/M phase reached 18.52%, 53.78%, and 53.74%, respectively (compared to 5.27% in DMSO-treated cells) (Fig. 2G and H and Supporting Information Fig. S4A). The significant G2/M phase arrest of the cell cycle observed demonstrated that NB1 could strongly regulate mitotic progression, consistent with the results of the RNA-Seq analysis.

Next, we checked the effect of NB1 on cell apoptosis. As depicted in Fig. 2I, NB1 time-dependently increased cleaved PARP protein. Further, Annexin V-FITC/PI staining was utilized to assess whether NB1 induced cell apoptosis in a dose-dependent manner. The results showed that NB1 treatment dose-dependently increased apoptosis cells. As shown in Fig. 2J and Fig. S4B, NB1 (15.6, 62.5, and 250.0 nmol/L) dose-dependently induced an increase (8.63%, 17.04%, and 41.10%) of apoptotic cells in MDA-MB-231 cells compared the DMSO-treated group (5.70% apoptosis cells). Similarly, there was a significant increase (7.80%−16.29%) of apoptotic cells in A549 cells after treating 500.0 nmol/L NB1 (Fig. 2K and Fig. S4B). Simultaneously, NB1 dose-dependently elevated cleaved PARP (an apoptosis marker) and reduced two anti-apoptosis factors, Bcl-2 and Mcl-1 (Fig. 2L). Together, NB1 significantly induced cell apoptosis in MDA-MB-231 and A549 cells.

2.5. *NB1 exerts Nur77-mediated anticancer activities by inducing Nur77 mitochondrial localization and activating Nur77/Bcl-2 apoptosis pathway*

Since NB1 was an excellent Nur77 ligand that effectively prompted mitotic arrest and apoptosis in cancer cells, we conducted a small interfering RNA (siNur77)-mediated knockdown assay to investigate whether the anticancer action of NB1 depended on Nur77. Fig. 3A showed the protein expression of Nur77 significantly decreased in A549-siNur77 cells compared to A549-siCtr (A549 cells transfected with siControl) cells. Nur77 deficiency could substantially attenuate the effect of NB1 blocking the cell cycle (Fig. 3B and Fig. S4C). NB1 treatment at 31.3 and 125.0 nmol/L resulted in 44.22% and 90.36% cells in the G2/M phase in A549-siCtr cells, respectively. However, NB1 at 31.3 and 125.0 nmol/L only caused 26.64% and 62.11% cells in the G2/M phase in A549-siNur77 cells. Consistently, NB1 strongly increased the apoptotic marker cleaved-PARP in A549-siCtr cells, which was significantly relieved in A549-siNur77 cells (Fig. 3C). Nur77 knockdown resulted in a significant decrease of NB1's antiproliferative activity against A549 cells, with IC_{50} from 91.9 ± 7.4 nmol/L (A549-siCtr) to 381.3 ± 1.9 nmol/L (A549-siNur77) (Fig. 3D). Similarly, NB1 showed better inhibition on HeLa-siCtr cells (IC_{50} = 70.7 ± 11.3 nmol/L) than HeLa-siNur77 cells (IC_{50} = 309.8 ± 0.8 nmol/L) (Fig. S4D and E). These results suggest that the inhibition of NB1 on cancer cells significantly depends on Nur77-mediated cell apoptosis.

Increasingly, studies have substantiated that Nur77 nuclear export is a critical step in Nur77-mediated apoptosis[20,31,33,37]. Thus, we investigated whether NB1 inhibited cell proliferation by modulating Nur77's nuclear translocation. As depicted in Fig. 3E, Nur77 was predominantly concentrated on the nucleus in DMSO-treated MDA-MB-231 cells, while NB1 stimulation led to a cytoplasmic distribution of Nur77. Also, the cellular fractionation assay demonstrated that NB1 effectively increased the content of Nur77 in the cytoplasm (Fig. 3F). Importantly, the antiproliferative activity of NB1 was significantly reversed by the specific nuclear export inhibitor Leptomycin B (LMB) with a significant increase of IC_{50} value (from 134.6 ± 3.2 to 302.5 ± 11.3 nmol/L) (Fig. 3G).

It is well-established that Nur77 can translocate to mitochondria and interact with Bcl-2, transforming the Bcl-2 configuration from an anti-apoptotic protein to a pro-apoptotic protein, ultimately inducing cell apoptosis[20,31]. Therefore, we further checked whether NB1 induced Nur77 mitochondrial-targeting and mitochondrion-related apoptosis. The immunofluorescence assay confirmed the ability of NB1 to promote the co-localization of Nur77 and mito-tracker (the specific probe of mitochondria) outside the nucleus (Fig. 3H). Moreover, the mitochondrial components isolating assay validated that NB1 could increase the enrichment of Nur77 on mitochondria (Fig. 3I). It implied that NB1 induced the translocation of Nur77 from the nucleus to the mitochondria. Then, we examined whether NB1 could induce the interaction of Nur77 and Bcl-2. The immunofluorescence assay showed that NB1 promoted an apparent co-localization of Nur77 with Bcl-2 at mitochondria (Fig. 3J). Furthermore, the co-immunoprecipitation (co-IP) assay demonstrated that NB1 could enhance Nur77 interaction with Bcl-2 (Fig. 3K). Together, NB1 might induce mitochondria-related apoptosis by the Nur77/Bcl-2 axis.

2.6. *NB1 prompted mitochondrion-related apoptosis*

The loss of mitochondrial membrane potential (MMP, $\Delta\psi$m) is a characteristic of mitochondria-related cell apoptosis. Herein, we utilized JC-1 (a specific MMP dye)[43] to monitor changes in MMP in MDA-MB-231 cells upon NB1 treatment. As shown in Fig. 4A and B, NB1 dose-dependently caused a significant loss of $\Delta\psi$m in MDA-MB-231 cells. The loss of $\Delta\psi$m in MDA-MB-231 cells exposed to NB1 at concentrations of 15.6, 62.5, and 250.0 nmol/L was 12.1%, 29.5%, and 31.4%, respectively. Moreover, NB1 induced the loss of $\Delta\psi$m in a Nur77-dependent manner. As shown in Fig. 4C and D and Fig. S4F, 31.3 nmol/L NB1 could cause 14.1% of $\Delta\psi$m loss in A549-siCtr cells, significantly higher than

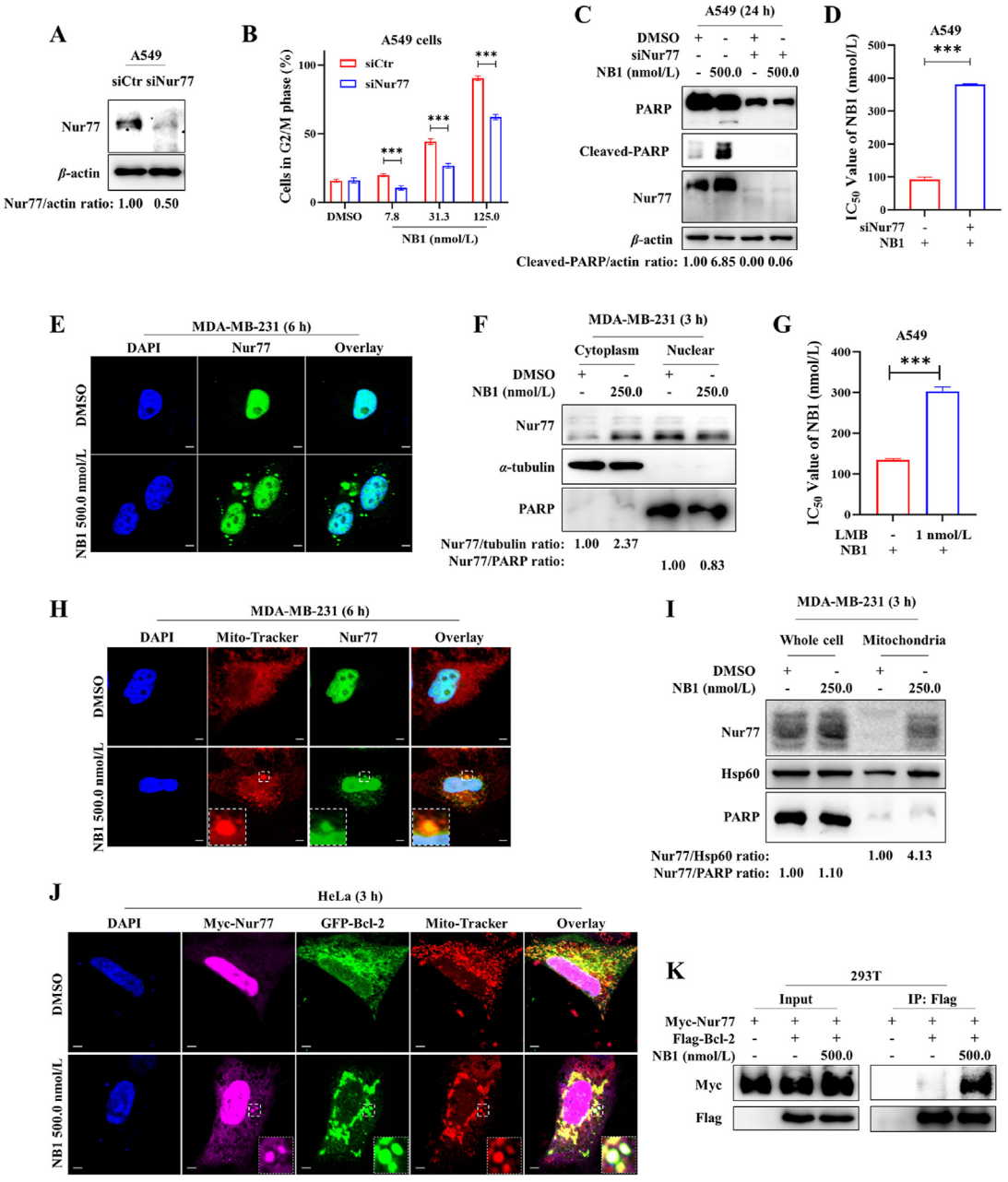

Figure 3 The inhibition of NB1 on cancer cells was dependent on Nur77/Bcl-2 apoptosis pathway. (A) A549 cells transfected with siControl (siCtr) or siNur77, then Western blot detected the Nur77 protein expression. (B) Quantitative analysis of relative cell number in G2/M phase in A549-siCtr and A549-siNur77 cells. A549-siCtr and A549-siNur77 cells were treated with NB1 at the indicated concentrations for 12 h, and the cell cycle was analyzed by flow cytometer. (C) Western blot examination of A549-siCtr and A549-siNur77 cells treated with NB1 at 500.0 nmol/L for 24 h. (D) MTT assay determined the IC_{50} of NB1 on A549-siCtr or A549-siNur77 cells at 72 h. (E) The subcellular localization of Nur77 in MDA-MB-231 cells was determined through an immunofluorescence assay following a 6-h treatment with NB1. Scale bar, 10 μm. (F) MDA-MB-231 cells were exposed to 250.0 nmol/L NB1 for 3 h. Nuclear and cytoplasmic fractions were extracted and analyzed by Western blot. (G) A549 cells were treated with NB1 with or without 1 nmol/L LMB. After 72 h, the cell viability was determined by MTT assay. (H) MDA-MB-231 cells were exposed to 500.0 nmol/L NB1 for 6 h and then probed with the Nur77 antibody and Mito-tracker. Scale bar, 10 μm. (I) NB1 induces the accumulation of Nur77 at mitochondria. Whole-cell lysates and mitochondrial fractions prepared from MDA-MB-231 cells treated with 250.0 nmol/L NB1 were analyzed by Western blot. (J) HeLa cells co-transfected with GFP-Bcl-2 and Myc-Nur77 plasmids were treated with 500.0 nmol/L NB1 for 3 h, and cells were incubated with mito-tracker and marked by Nur77 antibody and imaged by confocal microscopy. Scale bar, 10 μm. (K) 293T cells co-transfected with Myc-Nur77 and Flag-Bcl-2 for 24 h were treated with 500.0 nmol/L NB1 for 3 h. The interaction between Nur77 and Bcl-2 was analyzed using co-IP and Western blot assays. Data are shown as mean ± SD. ***$P < 0.001$ *vs.* control (siCtr or DMSO).

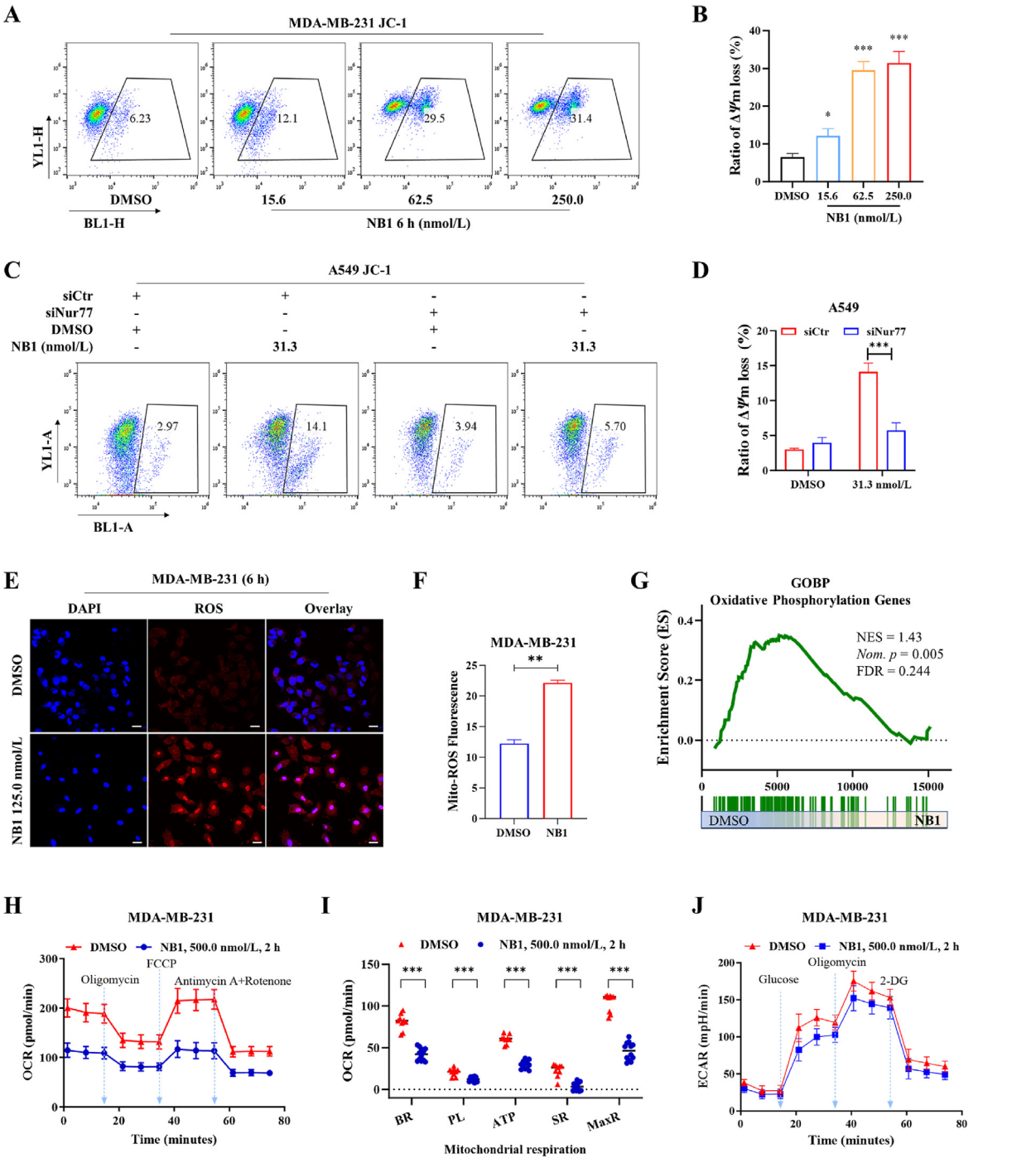

Figure 4 NB1 induced mitochondria-related apoptosis and caused a decrease in mitochondrial respiration. (A) MDA-MB-231 cells treated with the indicated concentration of NB1 for 6 h were incubated with JC-1, and then JC-1 fluorescence was measured by flow cytometry. (B) The ratio of Δψm loss induced by NB1 in (A). (C) A549-siCtr and A549-siNur77 cells treated with 31.3 nmol/L NB1 for 6 h were incubated with JC-1, and then JC-1 fluorescence was measured by flow cytometry. (D) The ratio of Δψm loss induced by NB1 in (C). (E) MDA-MB-231 cells treated with the 125.0 nmol/L NB1 for 6 h were incubated with Mito-ROS, and then cells were observed by confocal microscopy. Scale bar, 50 μm. (F) Quantification of fluorescence in (E). (G) GSEA analyzed the influence of NB1 on the oxidative phosphorylation gene signature in MDA-MB-231 cells. (H, I) Kinetic profiles of OCR (H) and quantification of basal respiration, proton leak, ATP production, max respiration, and spare respiration from OCR (I) in MDA-MB-231 cells after treating with 500.0 nmol/L NB1 for 2 h. (J) Glycolytic profiles of ECAR after treatment with 500.0 nmol/L NB1 for 2 h. Data are shown as mean ± SD. ns, not significant, $0.01 < {}^{*}P < 0.05$, $0.001 < {}^{**}P < 0.01$, ${}^{***}P < 0.001$ *vs.* control (DMSO).

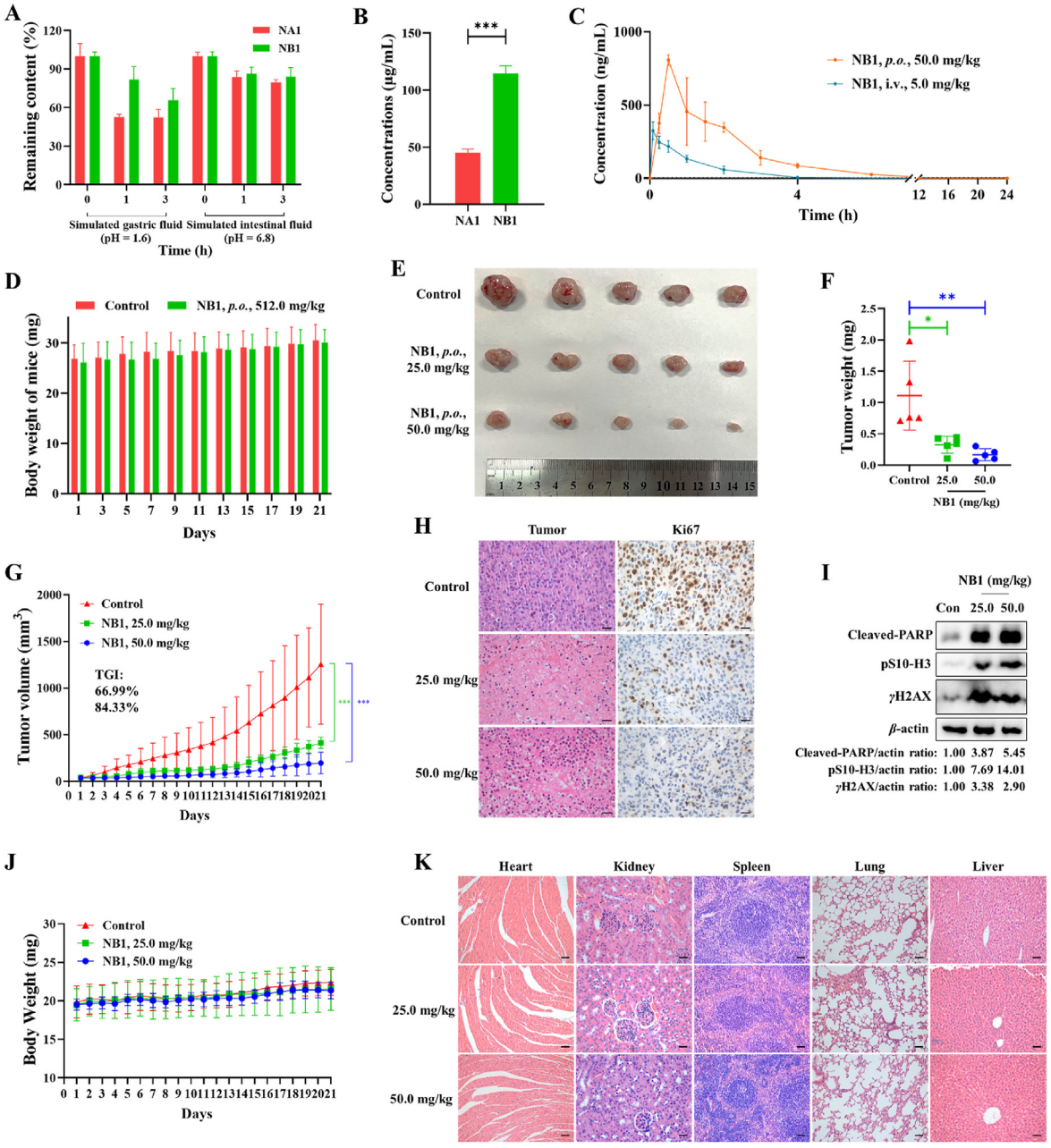

Figure 5 Preliminary druggability evaluation of NB1. (A) Stability experiments of compounds NA1 and NB1 in simulated gastric juice (pH = 1.6) and simulated intestinal juice (pH = 6.8). (B) Aqueous solubility of NA1 and NB1. (C) Drug-time concentration curves of NB1 after oral administration (*p.o.*) and intravenous injection (i.v.) in SD rats. (D) The effect of NB1 on body weight of female mice. (E, F) Nude mice ($n = 5$) injected with MDA-MB-231 (1×10^6 cells) were orally administrated 25.0 and 50.0 mg/kg NB1 once a day. After administration of NB1 for 21 days, nude mice were sacrificed, then tumors were removed, photographed (E), and weighed (F). (G) The change of tumor volume during the whole treatment cycle. (H) H&E and Ki67 staining of tumor tissues in the control and NB1-treated groups. Scale bar, 50 μm. (I) The expression of Cleaved-PARP, pS10-H3, and γH2AX in tumor specimens from MDA-MB-231 xenograft mice treated with or without NB1. (J) The change of mice weight during the whole treatment cycle. (K) H&E staining images of the major organs. The scale bar is 50 μm. Data are shown as mean ± SD. $0.01 < *P < 0.05$, $0.001 < **P < 0.01$, $***P < 0.001$ *vs.* control.

5.7% in A549-siNur77 cells. Also, the elevation of intracellular mitochondrial reactive oxygen species (Mito-ROS, another hallmark of mitochondrial dysfunction) was distinctly observed in MDA-MB-231 cells upon exposure to NB1 (Fig. 4E and F). Collectively, NB1 induced apoptosis in cancer cells through mitochondrion-related mechanisms.

Mitochondria, often called cell powerhouses, play a crucial role in regulating the metabolic state of cells[44,45]. GSEA revealed NB1 treatment led to a reduction of mitochondrion-related gene signatures in MDA-MB-231 cells, like Oxidative Phosphorylation (Fig. 4G), Inner Mitochondrial Membrane Protein Complex, and Tricarboxylic Acid Cycle genes (Supporting Information Fig. S5A and B). The mitochondrial dysfunction caused by NB1 might interrupt the bio-energetic support for cancer cells and even result in their starvation-induced demise[46]. Thus, we initiated a Seahorse® metabolic flux analysis to evaluate the mitochondrial respiration in

MDA-MB-231 cells, which were treated with DMSO or 500.0 nmol/L NB1 for 2 h. The oxygen consumption rate (OCR) was measured to assess the level of oxidative phosphorylation (OXPHOS) characterized by multiple critical parameters of mitochondrial function, including basal respiration (BR), proton leak (PL), ATP production (ATP), maximum respiration (MaxR), and spare respiratory capacity (SRC). The overall OCR profiles and specific changes in response to NB1 stimulation were depicted in Fig. 4H and I. In comparison to DMSO-treated cells, the NB1-treated cells exhibited a significant reduction of 48.2% in basal respiration, 39.9% in proton leak, 51.0% in ATP production, 56.0% in maximal respiration, and 83.5% in spare respiration. However, when glycolytic function was estimated by measuring extracellular acidification rate (ECAR), the results demonstrated that glycolytic capacity in MDA-MB-231 cells treated with NB1 had no significant difference from the control (Fig. 4J). Together, these data suggested that NB1 selectively suppressed OXPHOS but not glycolysis.

2.7. *Evaluation of the chemical stability and aqueous solubility of NB1*

Chemical stability and aqueous solubility are two critical physicochemical parameters of small molecules and are mainly responsible for the poor performance of active pharmaceutical ingredients during drug discovery and beyond. Herein, the chemical stability of compound NB1 and the lead NA1 was assessed in simulated gastric fluid (SGF) and simulated intestinal fluid (SIF). As shown in Fig. 5A, NB1 was more stable in SGF and SIF conditions than the lead NA1. Moreover, NB1 presented better aqueous solubility (pH = 7.4) than the lead NA1 (45.32 ± 3.01 μg/mL). In comparison with NA1, NB1 significantly increased the aqueous solubility by approximately 2.53 times, with a maximum dissolved concentration of about 114.63 ± 6.79 μg/mL (Fig. 5B). Given the good aqueous solubility and chemical stability, the potent Nur77 binder NB1 may be a promising oral anticancer agent.

2.8. *Pharmacokinetics analysis*

The pharmacokinetics (PK) profiles of NB1 were extensively studied in Sprague−Dawley (SD) rats by intravenous injection (i.v., 5.0 mg/kg) and oral administration (*p.o.*, 50.0 mg/kg). As shown in Fig. 5C, the plasma concentrations of each compound were monitored for 24 h. The related PK data were calculated and shown in Supporting Information Table S6. For the i.v. administration of 5.0 mg/kg NB1, the area under the concentration−time curve ($AUC_{0-\infty}$) was about 374.80 μg/L × h with a half-life ($t_{1/2}$) of 0.47 h, and the maximum plasma concentration (C_{max}) was 324.32 μg/L. For the *p.o.* administration (50.0 mg/kg), NB1 was rapidly adsorbed (T_{max} = 0.5 h), resulting in good oral exposure with an $AUC_{0-\infty}$ of 1397.85 μg/L × h, $t_{1/2}$ of 0.48 h, and C_{max} of 807.49 μg/L. The bioavailability (F) was about 38.5%, indicating the orally available property of NB1. Therefore, the *p.o.* administration was processed to evaluate the acute toxicity and therapeutic effects of NB1.

2.9. *Acute toxicity assay*

To assess the safety of NB1, a single dose administration was conducted in female KM mice *via* an oral (512.0 mg/kg) route. The *p.o.* administration of 512.0 mg/kg NB1 did not result in any fatalities. Besides, no notable weight loss or physical abnormalities were observed throughout a period of 21 days after NB1 administration (Fig. 5D). Furthermore, the effect of NB1 on five main organs (heart, spleen, kidney, liver, and lung) was also detected using hematoxylin and eosin (H&E). The H&E showed no significant morphological changes or abnormalities in these tissues (Supporting Information Fig. S6). Together, the oral toxicity of NB1 was low.

2.10. *In vivo anticancer activity*

As a potent Nur77 ligand, NB1 significantly inhibits various cancer lines *in vitro* (especially TNBC cell line MDA-MB-231, IC_{50} = 0.0030 ± 0.0015 μmol/L). TNBC is an aggressive histological subtype of breast cancer with a high risk of recurrence and metastasis and has a low 5-year survival rate due to its rapid drug resistance and lack of targeted therapy. Small molecules targeting Nur77 have been demonstrated as a promising treatment approach for TNBC[7,34,40]. Therefore, we examined the *in vivo* anticancer efficiency of NB1 in the MDA-MB-231 xenograft nude mice model. Fifteen female nude mice possessing MDA-MB-231 tumor xenografts were randomly divided into three groups for oral administration of vehicle, 25.0 mg/kg NB1, and 50.0 mg/kg NB1 once daily for 21 consecutive days, respectively. As observed in Fig. 5E and F, NB1 exhibited remarkable anticancer efficacies in both high- and low-dose treatment groups with TGI values of 66.99% (25.0 mg/kg) and 84.33% (50.0 mg/kg), respectively. Meanwhile, NB1 administration significantly lowered the tumor growth rate (Fig. 5G) in a time-dependent manner. Additionally, NB1 administration caused apparent nuclear shrinkage in tumor tissues and significantly suppressed the expression of the cell proliferation marker Ki67 (Fig. 5H). Western blot experiments showed that NB1 remarkably induced apoptosis (cleaved-PARP), mitotic arrest (pS10-H3), and DNA damage (γH2AX) in tumor tissues like the *in vitro* study (Fig. 5I). Excitingly, NB1 did not cause apparent body weight loss (Fig. 5J) during treatment. Simultaneously, H&E staining analysis demonstrated that NB1 treatment did not inflict any evident tissue damage to the main organs, including the heart, kidney, spleen, lung, and liver (Fig. 5K). These results demonstrated that NB1 exerts a potent anticancer effect and good animal safety.

3. Conclusions

Nur77 has been demonstrated to be involved in the progression of multiple tumors[14,47-49], and targeting Nur77 translocation has emerged as a highly promising therapeutic strategy against tumors[9,24,31,33]. Several Nur77 ligands with excellent anticancer activity have been identified as potentially binding to druggable binding site B. However, no co-crystal structure of an effective anticancer agent at Nur77 site B has been released. Also, there is an urgent shortage of Nur77 site B ligands with favorable drug properties. These problems hinder the therapeutic potential and the clinical agents of Nur77.

In the present work, anticancer compound BPA-B9 (NA1) bearing good Nur77-binding affinity at the binding site B was first obtained based on our in-house compound library screening. Then, we designed and optimized the chemical structure of NA1 using rational structure-based drug design. Among synthesized compounds, NB1 displayed excellent Nur77-binding activity ($K_{D\,(Nur77)}$ = 0.121 μmol/L), superior to other tested nuclear receptors (SI ≥ 6.5). Furthermore, we innovatively obtained the X-ray crystal structure of NB1 and $Nur77^{LBD}$ complex, which might be the first co-crystal of the functional molecule at $Nur77^{LBD}$ site B. Interestingly, NB1's binding mode and

interactions at Nur77^{LBD} site B differ significantly from those of TMPA (a non-functional molecule of the Nur77^{LBD} site B previously reported)[41]. Notably, NB1 significantly inhibited the cell proliferation of various cancer cell lines by dose-dependently inducing mitotic arrest and cell apoptosis. NB1 could translocate Nur77 from nuclear to mitochondrial and promote Nur77/Bcl-2 interaction to induce apoptosis, accompanied by mitochondrial dysfunction and mitochondrial respiration suppression in MDA-MB-231 cells. Furthermore, NB1 exhibited favorable safety and desirable PK profiles with excellent peak concentrations, *in vivo* exposures, and oral bioavailabilities (F = 38.5%). More importantly, NB1 displayed potent anticancer efficiencies in the MDA-MB-231 cell-derived tumor xenograft model. Together, NB1 could be a valuable Nur77-targeted anticancer drug candidate for further clinical development to treat various human cancers such as TNBC, lung cancer, cervical cancer, hepatocellular carcinoma, and so on.

Acknowledgments

This work was supported by grants from the National High Level Hospital Clinical Research Funding & Elite Medical Professionals Project of China-Japan Friendship Hospital (2023-NHLHCRF-DJMS-03 & NO.ZRJY2023-GG07), the Fundamental Research Funds for the Central Universities of China (20720180051 and 3332023095), the National Key Research and Development Program of China (2022YFF0710803 and 2022YFF0710800), the Joint Research Project of Fujian Provincial Health Commission and Fujian Department of Education (#2019-WJ-39, China), the National Natural Science Foundation of China (82300051), and Fujian Provincial Health Commission (#2021zylc29, China). The authors thank Cuiling Sun, Rong Ding, Junjie Chen, Yingpu Tian, and Ye Yun (Analysis and Measurement Center, School of Pharmaceutical Sciences, Xiamen University) for their help on the NMR test, HRMS analysis, SPR assay, flow cytometry assay, and confocal laser scanning microscope analysis, respectively. The authors also thank the staff at BL18U1/BL10U2 beamlines at SSRF of the National Facility for Protein Science in Shanghai (NFPS), Shanghai Advanced Research Institute, Chinese Academy of Sciences, for providing technical support in X-ray diffraction data collection and analysis.

Author contributions

Jun Chen: Writing − original draft, Visualization, Validation, Methodology, Investigation, Formal analysis, Data curation. Taige Zhao: Writing − original draft, Visualization, Validation, Methodology, Investigation, Formal analysis, Data curation. Wenbin Hong: Visualization, Methodology, Investigation, Formal analysis, Data curation. Hongsheng Li: Visualization, Formal analysis, Data curation. Mingtao Ao: Investigation. Yijing Zhong: Investigation. Xiaoya Chen: Investigation. Yingkun Qiu: Resources. Xiumin Wang: Resources. Zhen Wu: Resources. Tianwei Lin: Resources. Baicun Li: Supervision, Funding acquisition. Xueqin Chen: Supervision, Funding acquisition. Meijuan Fang: Writing − review & editing, Supervision, Project administration, Funding acquisition, Conceptualization.

Conflicts of interest

The authors have no conflicts of interest to declare.

Appendix A. Supporting information

Supporting information to this article can be found online at https://doi.org/10.1016/j.apsb.2024.07.012.

References

1. Pissios P, Tzameli I, Kushner PJ, Moore DD. Dynamic stabilization of nuclear receptor ligand binding domains by hormone or corepressor binding. *Mol Cel* 2000;**6**:245−53.
2. Cao X, Liu W, Lin F, Li H, Kolluri SK, Lin B, et al. Retinoid X receptor regulates Nur77/TR3-dependent apoptosis [corrected] by modulating its nuclear export and mitochondrial targeting. *Mol Cel Biol* 2004;**24**:9705−25.
3. Germain P, Staels B, Dacquet C, Spedding M, Laudet V. Overview of nomenclature of nuclear receptors. *Pharmacol Rev* 2006;**58**:685−704.
4. Wang L, Zheng Y, Gao X, Liu Y, You X. Retinoid X receptor ligand regulates RXRα/Nur77-dependent apoptosis *via* modulating its nuclear export and mitochondrial targeting. *Int J Clin Exp Pathol* 2017;**10**:10770−80.
5. Hedrick E, Lee SO, Doddapaneni R, Singh M, Safe S. NR4A1 antagonists inhibit β1-integrin-dependent breast cancer cell migration. *Mol Cel Biol* 2023;**36**:1383−94.
6. Lee SO, Abdelrahim M, Yoon K, Chintharlapalli S, Papineni S, Kim K, et al. Inactivation of the orphan nuclear receptor TR3/Nur77 inhibits pancreatic cancer cell and tumor growth. *Cancer Res* 2010;**70**:6824−36.
7. Karki K, Wright GA, Mohankumar K, Jin UH, Zhang XH, Safe S. A bis-indole-derived NR4A1 antagonist induces PD-L1 degradation and enhances antitumor immunity. *Cancer Res* 2020;**80**:1011−23.
8. Guan YF, Huang QL, Ai YL, Chen QT, Zhao WX, Wang XM, et al. Nur77-activated lncRNA WFDC21P attenuates hepatocarcinogenesis *via* modulating glycolysis. *Oncogene* 2020;**39**:2408−23.
9. Lin B, Kolluri SK, Lin F, Liu W, Han YH, Cao X, et al. Conversion of Bcl-2 from protector to killer by interaction with nuclear orphan receptor Nur77/TR3. *Cell* 2004;**116**:527−40.
10. Zhang XK. Targeting Nur77 translocation. *Expert Opin Ther Targets* 2007;**11**:69−79.
11. Yang PB, Hou PP, Liu FY, Hong WB, Chen HZ, Sun XY, et al. Blocking PPARgamma interaction facilitates Nur77 interdiction of fatty acid uptake and suppresses breast cancer progression. *Proc Natl Acad Sci U S A* 2020;**117**:27412−22.
12. Lacey A, Rodrigues-Hoffman A, Safe S. PAX3-FOXO1A expression in rhabdomyosarcoma is driven by the targetable nuclear receptor NR4A1. *Cancer Res* 2017;**77**:732−41.
13. Mu X, Chang C. TR3 orphan nuclear receptor mediates apoptosis through up-regulating E2F1 in human prostate cancer LNCaP cells. *J Biol Chem* 2003;**278**:42840−5.
14. Hedrick E, Mohankumar K, Safe S. TGFbeta-induced lung cancer cell migration is NR4A1-dependent. *Mol Cancer Res* 2018;**16**:1991−2002.
15. Chen J, Lopez-Moyado IF, Seo H, Lio CJ, Hempleman LJ, Sekiya T, et al. NR4A transcription factors limit CAR T cell function in solid tumours. *Nature* 2019;**567**:530−4.
16. Qin L, Zhao D, Xu J, Ren X, Terwilliger EF, Parangi S, et al. The vascular permeabilizing factors histamine and serotonin induce angiogenesis through TR3/Nur77 and subsequently truncate it through thrombospondin-1. *Blood* 2013;**121**:2154−64.
17. Zeng H, Qin L, Zhao D, Tan X, Manseau EJ, Van Hoang M, et al. Orphan nuclear receptor TR3/Nur77 regulates VEGF-A-induced angiogenesis through its transcriptional activity. *J Exp Med* 2006;**203**:719−29.
18. Chen C, Li Y, Hou S, Bourbon PM, Qin L, Zhao K, et al. Orphan nuclear receptor TR3/Nur77 biologics inhibit tumor growth by targeting angiogenesis and tumor cells. *Microvasc Res* 2020;**128**:103934.
19. Zhu B, Yang JR, Jia Y, Zhang P, Shen L, Li XL, et al. Overexpression of NR4A1 is associated with tumor recurrence and poor survival in non-small-cell lung carcinoma. *Oncotarget* 2017;**8**:113977−86.

20. Payapilly A, Guilbert R, Descamps T, White G, Magee P, Zhou C, et al. TIAM1-RAC1 promote small-cell lung cancer cell survival through antagonizing Nur77-induced BCL2 conformational change. *Cell Rep* 2021;**37**:109979.
21. Li X, Chen Q, Liu J, Lai S, Zhang M, Zhen T, et al. Orphan nuclear receptor Nur77 mediates the lethal endoplasmic reticulum stress and therapeutic efficacy of cryptomeridiol in hepatocellular carcinoma. *Cells* 2022;**11**:3870.
22. Liang B, Song X, Liu G, Li R, Xie J, Xiao L, et al. Involvement of TR3/Nur77 translocation to the endoplasmic reticulum in ER stress-induced apoptosis. *Exp Cel Res* 2007;**313**:2833−44.
23. Li B, Yao J, Guo K, He F, Chen K, Lin Z, et al. Design, synthesis, and biological evaluation of 5-((8-methoxy-2-methylquinolin-4-yl)amino)-1*H*-indole-2-carbohydrazide derivatives as novel Nur77 modulators. *Eur J Med Chem* 2020;**204**:112608.
24. Li H, Kolluri SK, Gu J, Dawson MI, Cao X, Hobbs PD, et al. Cytochrome c release and apoptosis induced by mitochondrial targeting of nuclear orphan receptor TR3. *Science* 2000;**289**:1159−64.
25. Zhan Y, Du X, Chen H, Liu J, Zhao B, Huang D, et al. Cytosporone B is an agonist for nuclear orphan receptor Nur77. *Nat Chem Biol* 2008;**4**:548−56.
26. Hu QY, Zhang XK, Wang JN, Chen HX, He LP, Tang JS, et al. Malayoside, a cardenolide glycoside extracted from *Antiaris toxicaria* Lesch, induces apoptosis in human non-small lung cancer cells *via* MAPK-Nur77 signaling pathway. *Biochem Pharmacol* 2021;**190**:114622.
27. Li B, Huang J, Liu J, He F, Wen F, Yang C, et al. Discovery of a Nur77-mediated cytoplasmic vacuolation and paraptosis inducer (4-PQBH) for the treatment of hepatocellular carcinoma. *Bioorg Chem* 2022;**121**:105651.
28. Li B, Yao J, He F, Liu J, Lin Z, Liu S, et al. Synthesis, SAR study, and bioactivity evaluation of a series of quinoline-indole-schiff base derivatives: compound **10E** as a new Nur77 exporter and autophagic death inducer. *Bioorg Chem* 2021;**113**:105008.
29. Ao M, Zhang J, Qian Y, Li B, Wang X, Chen J, et al. Design and synthesis of adamantyl-substituted flavonoid derivatives as anti-inflammatory Nur77 modulators: compound B7 targets Nur77 and improves LPS-induced inflammation *in vitro* and *in vivo*. *Bioorg Chem* 2022;**120**:105645.
30. Chen Z, Zhang D, Yan S, Hu C, Huang Z, Li Z, et al. SAR study of celastrol analogs targeting Nur77-mediated inflammatory pathway. *Eur J Med Chem* 2019;**177**:171−87.
31. Chen X, Cao X, Tu X, Alitongbieke G, Xia Z, Li X, et al. BI1071, a novel Nur77 modulator, induces apoptosis of cancer cells by activating the Nur77-Bcl-2 apoptotic pathway. *Mol Cancer Ther* 2019;**18**:886−99.
32. Hu M, Luo Q, Alitongbieke G, Chong S, Xu C, Xie L, et al. Celastrol-induced Nur77 interaction with TRAF2 alleviates inflammation by promoting mitochondrial ubiquitination and autophagy. *Mol Cel* 2017;**66**:141−53.
33. Qin J, Chen X, Liu W, Chen J, Liu W, Xia Y, et al. Discovery of 5-((4-(pyridin-3-yl)pyrimidin-2-yl)amino)-1*H*-indole-2-carboxamide derivatives as novel anti-cancer agents targeting Nur77. *Eur J Med Chem* 2022;**244**:114849.
34. Qin J, Niu B, Chen X, Hu C, Lu S, Li H, et al. Discovery of 5-(pyrimidin-2-ylamino)-1*H*-indole-2-carboxamide derivatives as Nur77 modulators with selective and potent activity against triple-negative breast cancer. *J Med Chem* 2023;**66**:15847−66.
35. Wang WJ, Wang Y, Chen HZ, Xing YZ, Li FW, Zhang Q, et al. Orphan nuclear receptor TR3 acts in autophagic cell death *via* mitochondrial signaling pathway. *Nat Chem Biol* 2014;**10**:133−40.
36. Liu M, Luo Z, Li Z, Lai X, Loh XJ, Wu C, et al. Engineered celastrol and plasmid co-delivery for *in situ* expression and targeted mitochondrial relocation of Nur77 protein towards effective drug resistance reversion. *Chem Eng J* 2023;**453**:139879.
37. He F, Chen J, Zhao T, Wu Q, Yin N, Wang X, et al. Design, synthesis, and evaluation of novel benzoylhydrazone derivatives as Nur77 modulators with potent antitumor activity against hepatocellular carcinoma. *J Enzyme Inhib Med Chem* 2023;**38**:2227777.
38. Xu Y, Wang S, Hu Q, Gao S, Ma X, Zhang W, et al. CavityPlus: a web server for protein cavity detection with pharmacophore modelling, allosteric site identification and covalent ligand binding ability prediction. *Nucleic Acids Res* 2018;**46**:W374−9.
39. Wang S, Xie J, Pei J, Lai L. CavityPlus 2022 update: an integrated platform for comprehensive protein cavity detection and property analyses with user-friendly tools and cavity databases. *J Mol Biol* 2023;**435**:168141.
40. Chen X, Gao M, Xia Y, Wang X, Qin J, He H, et al. Phase separation of Nur77 mediates XS561-induced apoptosis by promoting the formation of Nur77/Bcl-2 condensates. *Acta Pharm Sin B* 2024;**14**:1204−21.
41. Zhan YY, Chen Y, Zhang Q, Zhuang JJ, Tian M, Chen HZ, et al. The orphan nuclear receptor Nur77 regulates LKB1 localization and activates AMPK. *Nat Chem Biol* 2012;**8**:897−904.
42. Chen J, Zhao T, He F, Zhong Y, Wang S, Tang Z, et al. Discovery of bipyridine amide derivatives targeting pRXRalpha−PLK1 interaction for anticancer therapy. *Eur J Med Chem* 2023;**254**:115341.
43. Reers M, Smiley ST, Mottola-Hartshorn C, Chen A, Lin M, Chen LB. Mitochondrial membrane potential monitored by JC-1 dye. *Methods Enzymol* 1995;**260**:406−17.
44. Wallace DC. Mitochondria and cancer. *Nat Rev Cancer* 2012;**12**:685−98.
45. Kuang S, Sun L, Zhang X, Liao X, Rees TW, Zeng L, et al. A mitochondrion-localized two-photon photosensitizer generating carbon radicals against hypoxic tumors. *Angew Chem Int Ed Engl* 2020;**59**:20697−703.
46. Wang MM, Xu FJ, Su Y, Geng Y, Qian XT, Xue XL, et al. A new strategy to fight metallodrug resistance: mitochondria-relevant treatment through mitophagy to inhibit metabolic adaptations of cancer cells. *Angew Chem Int Ed Engl* 2022;**61**:e202203843.
47. To SKY, Zeng JZ, Wong AST. Nur77: a potential therapeutic target in cancer. *Expert Opin Ther Targets* 2012;**16**:573−85.
48. Li XX, Wang ZJ, Zheng Y, Guan YF, Yang PB, Chen X, et al. Nuclear receptor Nur77 facilitates melanoma cell survival under metabolic stress by protecting fatty acid oxidation. *Mol Cel* 2018;**69**:480−92.
49. Guo H, Golczer G, Wittner BS, Langenbucher A, Zachariah M, Dubash TD, et al. NR4A1 regulates expression of immediate early genes, suppressing replication stress in cancer. *Mol Cel* 2021;**81**:4041−4058 e15.